Bouncing, coalescence, and separation in head-on collision of unequal-size droplets

Chenglong Tang, Peng Zhang, and Chung K. Law

Citation: Phys. Fluids **24**, 022101 (2012); doi: 10.1063/1.3679165
View online: http://dx.doi.org/10.1063/1.3679165
View Table of Contents: http://pof.aip.org/resource/1/PHFLE6/v24/i2
Published by the American Institute of Physics.

Bouncing, coalescence, and separation in head-on collision of unequal-size droplets

Chenglong Tang,[a] Peng Zhang, and Chung K. Law[b]
Department of Mechanical and Aerospace Engineering, Princeton University, Princeton, New Jersey 08544, USA

(Received 10 April 2011; accepted 3 January 2012; published online 1 February 2012)

The dynamics of head-on collision of unequal-size droplets were experimentally and theoretically investigated, with emphasis on identifying distinct collision outcomes and interpreting the size-ratio dependence. A unified regime diagram in terms of bouncing, permanent coalescence, and separation after coalescence was identified for hydrocarbon and water droplets in the parameter space of the size ratio and a collision Weber number. Experimental results show that the transition Weber number, $We_{b\text{-}c}$, that separates the bouncing and permanent coalescence regimes, weakly depends on the size ratio, while the transition Weber number, $We_{c\text{-}s}$, that separates permanent coalescence and separation regimes, significantly increases with the size ratio. A theoretical model based on energy balance and scaling analysis was developed to explain the size-ratio dependence of $We_{c\text{-}s}$. The theoretical results show good agreement with the experimental data for tetradecane and decane droplets, with a moderate discrepancy for water droplets. © *2012 American Institute of Physics*. [doi:10.1063/1.3679165]

I. INTRODUCTION

The dynamics of droplet collision is relevant to many phenomena in nature such as the raindrop formation,[1,2] ocean mist production,[3] and atmospheric aerosols circulation.[4] Droplet collision is also ubiquitous in many industrial processes, especially those involving spraying.[5] A prominent example is the propensity of droplet collision in the dense spray region downstream of the injector in diesel and rocket engines. The frequent collisions and subsequent coalescence and separation can significantly modify the size and velocity distributions of the droplets in the spray, which in turn affect the eventual combustor performance.[6]

Earlier experimental studies on droplet collision were focused on the binary collision of identical water droplets in atmospheric air.[1,7–9] These studies showed that, depending on the collision Weber number, *We*, which measures the relative importance of the translational kinetic energy and the surface energy of the droplets, and the impact parameter, *B*, which measures the deviation of the trajectory of the droplets from that of head-on impact, collision may result in either permanent coalescence or separation after temporary coalescence. Subsequent experiments on hydrocarbons by Jiang, Umemura, and Law[10] identified a bouncing regime in the *B*-*We* parameter space, which divides the permanent coalescence regime into two regimes, namely, a coalescence regime after small droplet deformation, compared with the original droplet size, and a coalescence regime with large deformation. Qian and Law[11] extended the study to include effects of ambient pressures that are either lower or higher than atmospheric, for both water and hydrocarbon droplets, and found that the bouncing regime can be recovered for water at elevated pressures and suppressed for hydrocarbons at reduced pressures. A refined regime diagram consisting of five distinct collision regimes was consequently identified in the parameter space of *B*-*We*: (I) permanent coalescence

[a]Present address: Xi'an Jiaotong University, Xi'an, China. Electronic mail: chenglongtang@mail.xjtu.edu.cn.
[b]Author to whom correspondence should be addressed. Electronic mail: cklaw@princeton.edu.

after small droplet deformation, (II) bouncing, (III) permanent coalescence after large deformation, (IV) near head-on separation after temporary coalescence, and (V) off-center separation after temporary coalescence.

Compared to the large number of investigations on the collision of identical droplets, relatively few studies have been conducted on unequal-size droplet collision. Brazier-Smith *et al.*[2] conducted experiments on water droplets of different sizes, and correlated the coalescence efficiency with the Weber number, which measures the dependence of the boundary between the coalescence and separation regimes on the impact parameter, with effects of size ratio empirically taken into account. Ashgriz and Poo.[12] experimented with water droplets of different sizes and derived an expression, based on the inviscid flow assumption, to correlate their experimental results on the transition Weber number separating the coalescence and separation regimes. More recently, Rabe *et al.*[13] extended Ashgriz's work by defining a "symmetric" Weber number, which consists of the size ratio, and derived a formula that correlated well their results as well as those of Ashgriz *et al.*

In the present study, we aim to extend the previous studies on unequal-size head-on droplet collision to liquids with a wide range of rheological properties, especially the liquid viscosity which as will be shown is an essential property governing the subject phenomena. We are particularly interested in identifying distinct collision outcomes and interpreting their size-ratio dependence on the dynamic and rheological aspects of the problem. On the practical side, we are interested to explore the potential of enhancing the ignition of gelled hypergolic propellants for rocket engines by exploiting the size differential in droplet collisions. Specifically, because of the low volatility of these propellants, ignition is likely initiated in the liquid phase upon the merging and mixing of the colliding fuel, oxidizer droplets, and jets. In order to facilitate ignition, it is therefore desirable to have the colliding liquid elements first merge, and then remain merged without further separation. In this regard we conjectured that unequal sized droplets hold the potential to enhance droplet coalescence based on the following reasoning. First, the droplet having a smaller size in the unequal-size pair has a larger capillary pressure to resist deformation. The reduced deformation and hence the smaller frontal area of the impacting surface would result in reduced repulsive force from the compressed gas flow between the droplets and consequently promote coalescence. Second, the droplet with the larger size has the potential to accommodate (through surface distortion) and dissipate (by internal motion) the excess kinetic energy carried by the smaller droplet and hence stabilize the coalesced droplet. Furthermore, equal-size droplet collision has minimal mixing upon droplet coalescence due to the symmetry with respect to the collision plane (the $z = 0$ plane in Figure 1(a)). Thus, breaking the symmetry through the droplet sizes could result in improved mixing upon coalescence and promote reaction of the hypergolic bipropellants.

In the following, we shall first show a series of time-resolved droplet collision images for the head-on collisions of unequal sized droplets, in Sec. II. In Sec. III the results are presented in a collision outcome regime diagram, which demonstrates and quantifies the facilitation of coalescence with increasing size differential. A theoretical model based on energy balance and scaling analysis is subsequently derived, in Sec. IV, that successfully describes the experimental results on the size-ratio dependence of the transition Weber number.

II. EXPERIMENTAL METHODOLOGY

The experimental apparatus and procedure employed in the present study are similar to those of Refs. 10 and 11, with the exception that the two streams of colliding droplets are independently generated and thereby controlled. Since one of the droplet generators is anchored in a three-dimensional positioner while the other can rotate in a vertical plane, the generated droplet streams can be directed against each other. By tuning the delay phase of the strobe light, which is synchronized with the droplet generation circuit, time-resolved images can be taken through photographically triggered by the pulse from the droplet generator. By flashing the strobe light twice within one pulse period, the camera can record exactly the same droplet with a short phase difference, allowing the droplet velocity to be determined.

In the present experiment, tetradecane, decane, and water were used for their distinct physical properties. Specifically, as shown in Table I, the viscosity of tetradecane is about twice that of decane

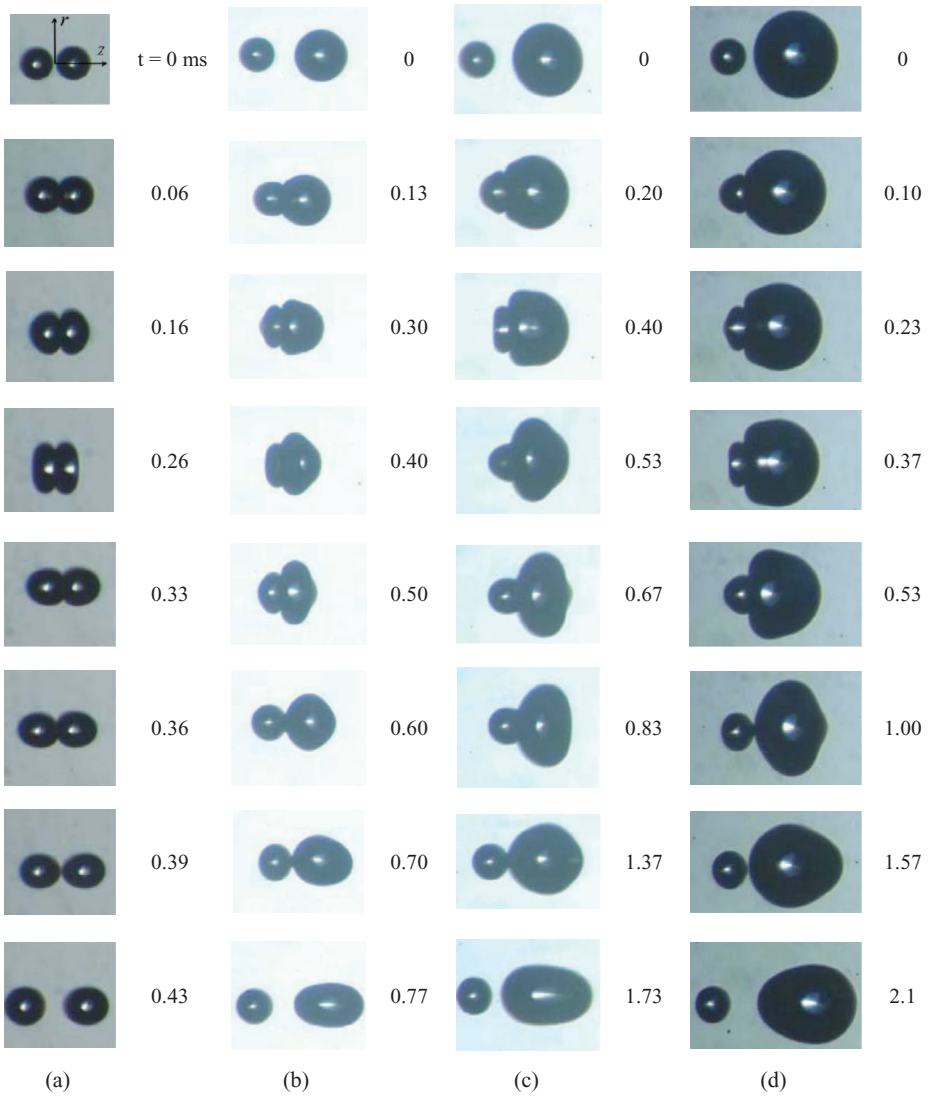

FIG. 1. (Color online) Photographic images showing representative bouncing collision sequences for tetradecane droplet collisions. (a) (We_s, Δ) = (8.5, 1.0); (b) (7.3, 1.46); (c) (7.3, 1.87); (d) (7.0, 2.33).

while they have similar surface tension. By the same token, while the viscosity of decane is similar to that of water, its surface tension is about one third of that of water. The radius of the smaller droplet was fixed at about 100 μm. Thus, by changing the nozzle size for the larger droplet generator, an unequal-size droplet pair can be realized.

We define the collision Weber number as $We_s = 2\rho R_s U^2/\sigma$, where ρ, R_s, and U are, respectively, the liquid density, radius of the small droplet, relative impact velocity, with the subscript "S" designating the smaller droplet. Furthermore, we shall use the size ratio, $\Delta = R_l/R_s = We_l/We_s$,

TABLE I. Properties of tested liquids.

Liquids	Surface tension, σ 10^{-2} N/m	Viscosity, μ 10^{-3} Ns/m^2	Density, ρ 10^3 kg/m^3
Water	7.29	1.0	1.0
Decane	2.38	0.92	0.73
Tetradecane	2.65	2.3	0.76

instead of the Weber number of the larger droplet, We_l, to complete the characterization of the dynamical aspect of the problem. For the equal-size situation, We_s degenerates to $We = 2\rho RU^2/\sigma$. Since viscous dissipation plays an essential role in droplet collision, we define the Ohnesorge number, $Z = 16\ \mu/\sqrt{\rho R_s \sigma}$ to measure the relative importance of viscosity compared to surface tension. In the present experiment, We_s varies from 5 to 90, Δ from 1.0 to 2.9, Z from 0.18 to 0.82, and Reynolds number (defined as $Re = \rho D_s U/\mu$) from around 100 to 1000.

III. EXPERIMENTAL OBSERVATIONS

A. Collision images and time sequences

As baseline for comparison, we first experimented with equal-size droplets. While we have experimented with all liquids, we shall only show the images of tetradecane droplets for illustration. Specifically, Figure 1(a) shows the bouncing case at $We_s = 8.5$, corresponding to Regime II. It is seen that, at $t = 0.26$ ms, the droplets have reached their maximum deformation in the r-direction, which is much larger than their initial sizes. Since coalescence does not occur, the droplets eventually bounce away from each other. Figure 2(a) shows the coalescence case at $We_s = 16.1$, corresponding

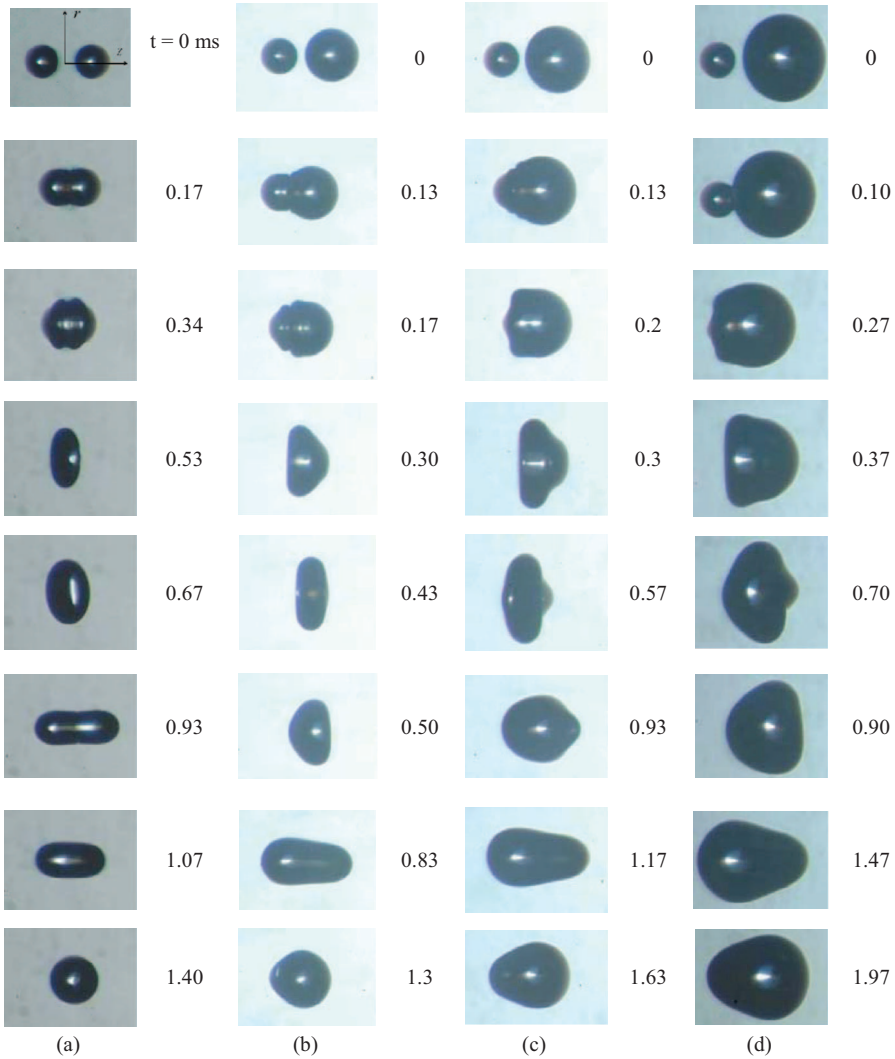

FIG. 2. (Color online) Photographic images showing representative coalescence collision sequences for tetradecane droplet collisions. (a) (We_s, Δ) = (16.1, 1.0); (b) (13.8, 1.46); (c) (17.6, 1.87); (d) (16.5, 2.33).

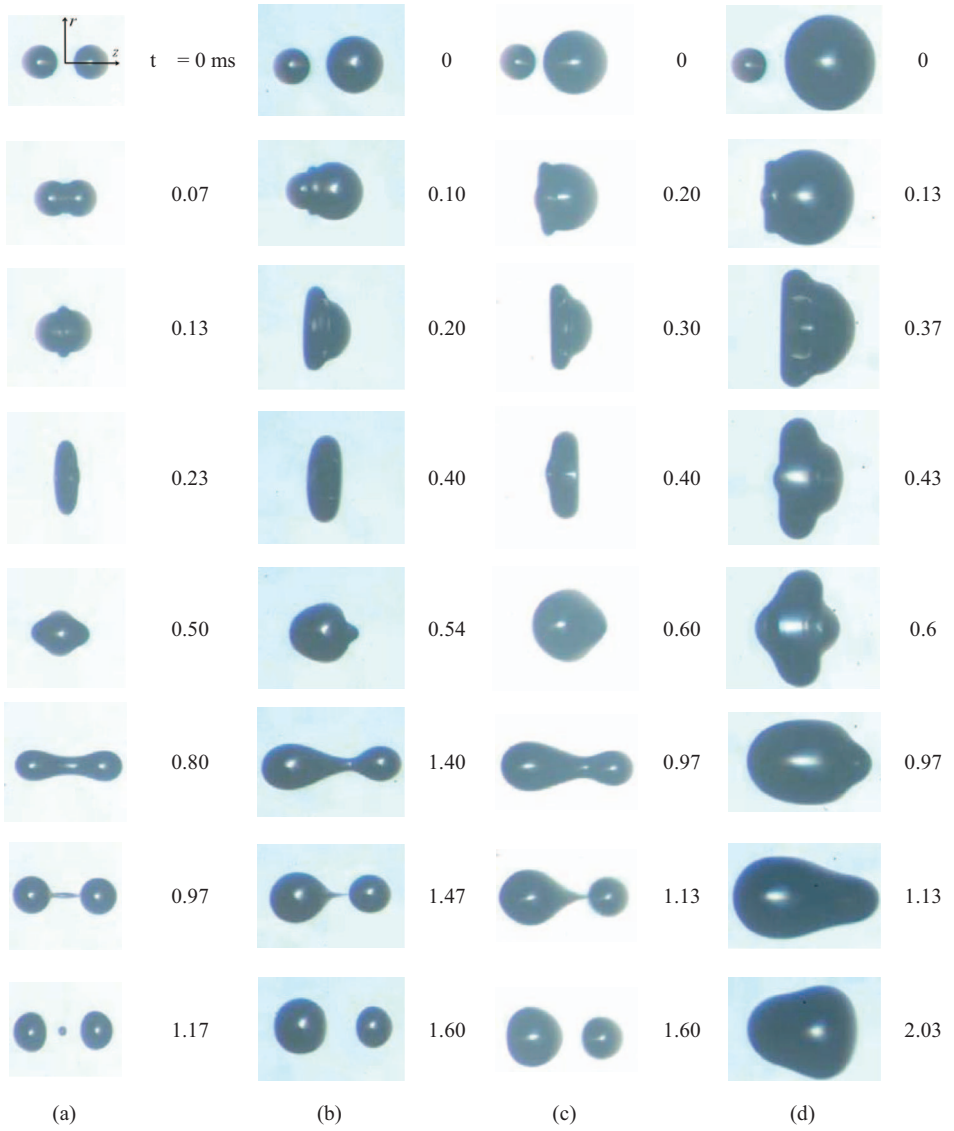

FIG. 3. (Color online) Photographic images showing representative separation collision sequences for tetradecane droplet collisions. (a) (We_s, Δ) = (39.1, 1.0); (b) (52.8, 1.50); (c) (58.8, 1.78); (d) (68.0, 2.50). Separation at $\Delta = 2.5$ was not observed up to $We_s = 68$.

to Regime III. The two droplets coalesce at $t = 0.34$ ms and the coalesced droplet reaches maximum deformation in the r-direction at $t = 0.53$ ms. Although further deformation in the z-direction tends to stretch the droplet to separate, as seen in the image at $t = 0.93$, separation eventually does not occur since viscous dissipation through the internal motion of the droplet reduces the available kinetic energy to separate the merged droplet.[10,11] Figure 3(a) shows the separation case at $We_s = 39.1$, corresponding to Regime IV. At such a large Weber number, the droplets undergo substantial deformation, as shown in the images at $t = 0.23$ and 0.80. Since the surface tension of the stretched droplet cannot hold the large amount of the kinetic energy associated with the internal motion, even with the stabilization effect of viscous dissipation, the merged droplet eventually separates and a smaller, satellite droplet is concomitantly formed. To compare with previous experiments,[11] the transition Weber numbers from Regime II to Regime III and to Regime IV were found to be 13.7 and 34 in the present experiments, which are almost identical to those reported in Ref. 11.

Similar to the equal-size situations, bouncing, coalescence, and separation were observed for unequal-size droplet collisions, as shown in Figures 1–3, respectively. Figures 1(b)–1(d) show the collision images for different size ratios but similar Weber numbers ($We_s = 7.0$–8.5). Under such situations, the droplets come into contact and experience moderate deformation and then bounce back. Unlike the equal-size case in which droplet deformation for each droplet is identical in space and time, the unequal-size droplets show different behaviors in response to the collision. First, the extent of deformation is different for the droplets because of their different capillary pressure $2\sigma/R$ to resist deformation. Second, the droplets reach their respective maximum deformations at different times. As shown in Figure 1(c), the larger droplet needs a longer time ($t = 0.67$ ms) to reach its maximum deformation in the r-direction than the smaller droplet does ($t = 0.4$ ms). The underlying physics is that the droplets have different characteristic response times, which is proportional to the natural oscillation time, $t_{osc} = (\rho R^3/\sigma)^{1/2}$, and is longer for the larger droplet. Many experimental observations have shown that the collision process usually occurs within a few droplet oscillation times for the Weber numbers of interest in the study.[10,11]

Figures 2(b)–2(d) show the coalescence cases for different size ratios but similar Weber number ($We_s = 13.8$–17.6). An interesting observation is that a rear-face bulge is formed on the coalesced droplet and the size of the bulge depends on the size ratio, as shown at $t = 0.3$ ms in Figure 2(b), at $t = 0.57$ ms in Figure 2(c), and $t = 0.7$ ms in Figure 2(d), respectively. The formation of the bulge is caused by the transfer of the kinetic energy of the smaller droplet to the larger one upon coalescence. The excess energy provides the momentum of the liquid element to push forward to cause separation, which, however, is suppressed due to the stabilizing effects of surface tension and viscous dissipation. The droplet therefore remains coalesced, with a bulge.

Figures 3(b)–3(d) show the separation cases for different size ratios. Separation is observed for the size ratios 1.5 and 1.78 but not for 2.5 even though the Weber number is larger for the $\Delta = 2.5$ case. This implies that increasing the size ratio suppresses droplet separation. Another interesting observation is that while a satellite droplet is formed after droplet separation for $\Delta = 1$, it is absent for $\Delta = 1.5$ and 1.78. The formation of satellite droplets is attributed to the capillary instability of the liquid bridge, as shown at $t = 0.97$ in Figure 3(a). For the unequal-size situations, because of the loss of symmetry, the liquid bridge tends to stick to the larger droplet instead of forming a satellite droplet.

B. Regime diagram in Δ-*We* space

Figure 4 shows the experimentally measured regime diagram in the parameter space of size ratio and Weber number, for tetradecane droplets. It is seen that, for a given size ratio, three different regimes were observed with increasing Weber number, namely, bouncing (Regime II), coalescence (Regime III), and separation after coalescence (Regime IV). The coalescence regime with small deformation (Regime I) is not shown in the regime diagram because it occurs in a narrow range of small Weber number ($We_s < 5$), which cannot be accurately quantified in the present study due to limitation of the experimentation.

The above mapping shows that the size ratio has only a moderately weak influence on the transition from Regime II to Regime III, and no distinct trend can be assessed from the data. The transition Weber number, $We_{b\text{-}c}$, varies in the range of 10.0–12.0 for the size ratios investigated herein. On the other hand, the size ratio significantly influences the boundary of subsequent droplet separation with further increase in the Weber number in that the coalescence regime (Regime III) is substantially extended with increasing size ratio. A distinct boundary separating Regime III and Regime IV can be readily seen in Figure 4 up to the size ratio $\Delta \approx 1.8$. At higher size ratios such as $\Delta = 2.6$, droplet separation was not observed up to $We_s \approx 70$. We could not generate temporally and spatially stable droplets for higher Weber numbers.

The regime diagram for decane droplet collision is similar to that of tetradecane, as shown in Figure 5. The critical Weber number $We_{b\text{-}c}$ is almost independent of the size ratio in the range of the size ratio studied, while $We_{c\text{-}s}$ again significantly increases with the size ratio. At $\Delta = 2.4$, separation was not observed up to $We_s = 50$.

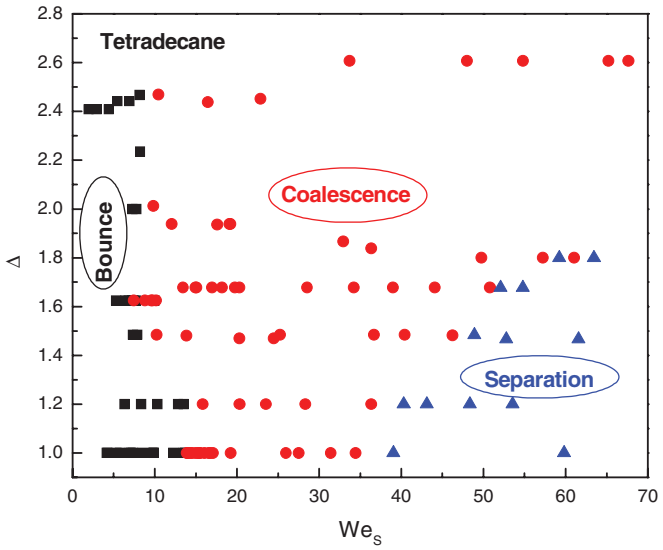

FIG. 4. (Color online) Experimentally identified regime diagram for tetradecane droplet collision.

The regime diagram for water droplet collision is shown for comparison in Figure 6. In the size ratio and Weber number range of interest, bouncing regime was not observed. This is consistent with the previous experimental observations.[7,11] It is seen that although $We_{c\text{-}s}$ of water also increases with the size ratio, the increase is not as significant as that for tetradecane and decane. The underlying physics is discussed in Sec. IV.

IV. CRITERION FOR COALESCENCE-SEPARATION TRANSITION

A. Theoretical model

For head-on collision of equal-size droplets, Qian and Law[11] developed a criterion based on energy balance for transition between coalescence and separation. In their analysis, the process of

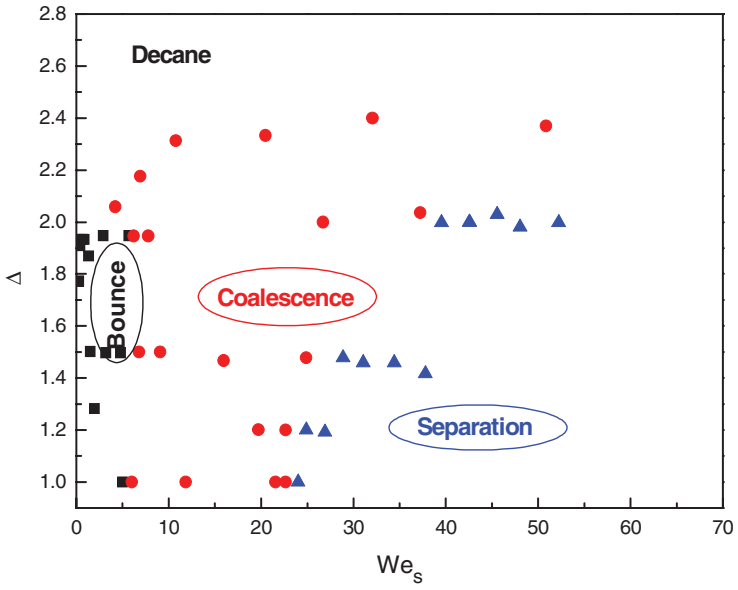

FIG. 5. (Color online) Experimentally measured regime diagram for decane droplet collision.

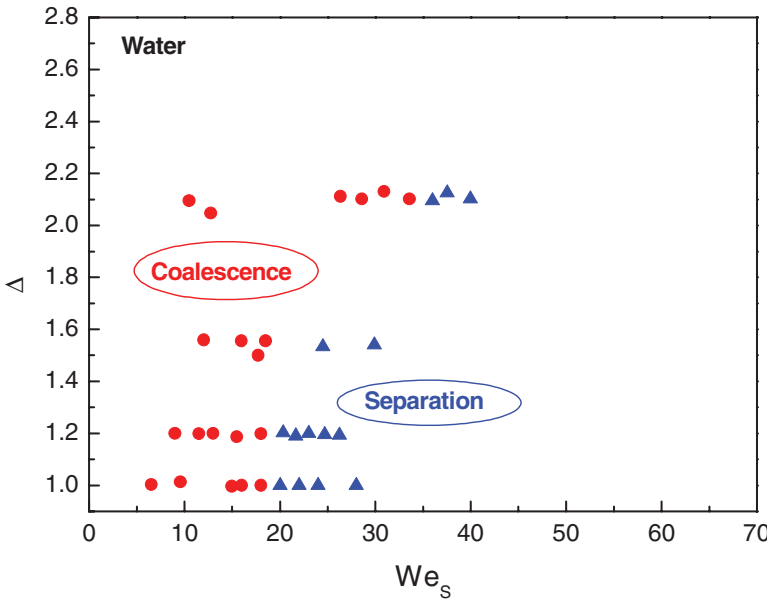

FIG. 6. (Color online) Experimentally measured regime diagram for water droplet collision.

separation was divided into three stages (Figure 11 in Ref. 11). Specifically, in Stage 1 the droplets first coalesce and then reach the maximum deformation in the r-direction. In Stage 2 the merged droplet contracts under surface tension attempting to recover the spherical shape. In Stage 3 a liquid cylinder is formed and is continuously stretched until it eventually breaks if there is enough internal kinetic energy.

For unequal-size droplet collision, the droplet deformation is more complex because of the loss of the symmetric shape. Nevertheless, we can still divide the process into three representative stages, which are schematically illustrated in Figure 7. In Stage 1, the merged droplet spreads outwardly in the r-direction to form a shape like a "flying saucer" (Instant 2). Compared to the equal-size situation, the merged droplet has a bulge on the side of the initially larger droplet as it reaches the maximum deformation (Instant 3). In Stage 2, the deformed droplet starts to contract at rim under the capillary pressure $\sigma(1/a + 1/b)$, while the bulge starts to spread outwardly under the capillary pressure, $2\sigma/c$. As a consequence, a new bulge was formed on the side of the initially smaller droplet while the bulge formed in Stage 1 completely disappears (Instant 4). The deformation continues until it eventually tends to a near-spherical shape (Instant 6). In Stage 3, a stretched asymmetrical liquid cylinder is formed (Instant 7) with both ends moving away from each other along the z-axis to form a liquid ligament (Instant 8), which eventually reaches a critical shape for incipient separation (Instant 9).

Energy conservation for the above process can be written as

$$E_{k0} + \sigma S_0 = \Phi_1 + \Phi_2 + \Phi_3 + E_{kf} + \sigma S_f, \tag{1}$$

where E_k and σS are, respectively, the total translational kinetic energy and surface energy of the colliding droplets, the subscripts "0" and "f," respectively, denote the initial time and the final state of separation.

Φ_1, Φ_2, and Φ_3 are, respectively, the total viscous loss during the three stages discussed above. In Qian and Law's analysis,[11] in order to determine the critical Weber number for the transition from coalescence to separation, the initial kinetic energy is assumed to be just large enough to overcome the viscous dissipation after coalescence and break the ligament. Based on this criterion, separation of the coalesced droplet depends on whether there is a residue kinetic energy E_{kf} at the critical point, which is given by

$$E_{kf} = E_{k0} - (\Phi_1 + \Phi_2 + \Phi_3) - \sigma(S_f - S_0). \tag{2}$$

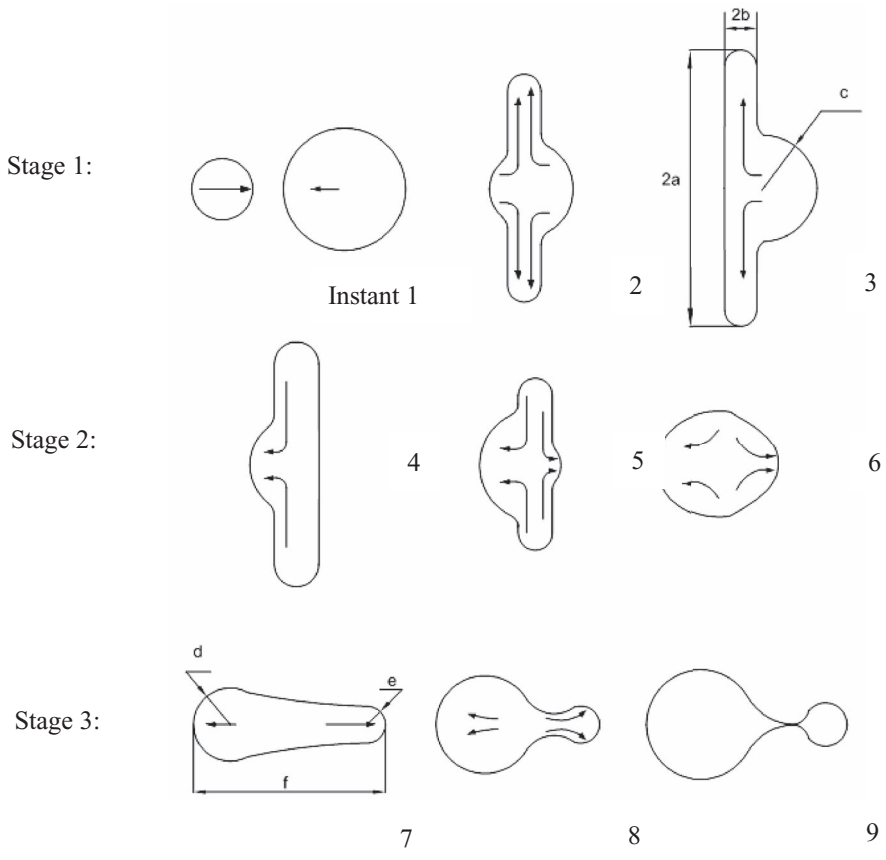

FIG. 7. Schematic of the three collision stages for unequal-size droplet collision.

Specifically, if $E_{kf} > 0$, the droplet has some residue kinetic energy to further stretch the ligament and hence effect the separation, otherwise the ligament will contract under surface tension and the droplet remains merged. Consequently, the critical Weber number, $We_{\text{c-s}}$, can be determined by the relation $E_{kf} = 0$, namely,

$$E_{k0} - (\Phi_1 + \Phi_2 + \Phi_3) - \sigma(S_f - S_0) = 0. \tag{3}$$

In order to establish an explicit criterion for $We_{\text{c-s}}$, we need to evaluate the viscous dissipation terms in Eq. (3), which is discussed next.

B. Evaluation of viscous dissipation in Stages 1–3

In order to determine accurately the cumulative viscous dissipation in the different stages of droplet collision, we need to know the unsteady flow field of the droplet internal motion and the evolution of the surface geometry, which can be obtained only by solving the 3D Navier-Stokes equation and using various numerical techniques for gas-liquid interface tracking.[14] Moreover, experimental measurement of the flow field within the 100 μm-size droplet is fundamentally challenging. We shall therefore develop an approximate evaluation of the viscous dissipation through simple scaling analysis.

To evaluate the viscous loss Φ_1, we can write the energy balance for Stage 1 as

$$E_{k0} + \sigma S_0 = \Phi_1 + \sigma S_1, \tag{4}$$

$$E_{k0} = \frac{1}{2}\left(\frac{4}{3}\rho\pi R_s^3 V_s^2 + \frac{4}{3}\rho\pi R_l^3 V_l^2\right) = \frac{\Delta^3 \pi R_s^2 \sigma}{3(1+\Delta^3)} We_s, \tag{5}$$

where V_s and V_l are respectively the velocities in the reference frame attached to the center of mass of the two-body system. The motion of the center of mass has no influence on the outcome of droplet collision and is negligibly small in the present experiments.

Following Jiang, Umemura, and Law,[10] we define a viscous loss coefficient α as

$$\Phi_1 = \alpha E_{k0} = \alpha \frac{\pi R_s^2 \sigma}{3(1+\Delta^{-3})} We_s, \tag{6}$$

and accordingly rewrite Eq. (4) as

$$S_1/S_0 = 1 + (1-\alpha) We_s^*, \tag{7}$$

where We_s^* is a modified Weber number of the smaller droplet, given by

$$We_s^* = \frac{E_{k0}}{\sigma S_0} = \frac{\Delta^3}{12(1+\Delta^3)(1+\Delta^2)} We_s. \tag{8}$$

It is noted that We_s^* is an important parameter that represents the ratio of overall kinetic energy over the surface energy. By approximating the coalesced droplet as a solid of revolution, we can measure S_1 for different Δ and We_s^*, as shown in Figure 8. It is seen that, for a given size ratio, S_1/S_0 can be closely correlated by a linear function of We_s^* and α can be subsequently determined by Eq. (7). The inset figure shows that α slightly increases with increasing size ratio, from 0.50 at $\Delta = 1$ to 0.56 at $\Delta = 1.8$. The result that about half of the initial kinetic energy is dissipated during droplet deformation in Stage 1 agrees with the previous result of Jiang *et al.*[10] By using Eq. (7) and the fitted α as a weak function of Δ, we can immediately conclude that the viscous loss in Stage 1 moderately increases with the size ratio for given We_s, R_s, and σ.

To evaluate Φ_2, we note that the capillary pressure that drives the flow in the disk-shape portion of the droplet, as shown in Instant 4 of Figure 7, is proportional to $\sigma(1/a + 1/b)$ and hence we can have the scaling relation

$$\frac{1}{2}\rho v_2^2 = \sigma\left(\frac{1}{a} + \frac{1}{b}\right), \tag{9}$$

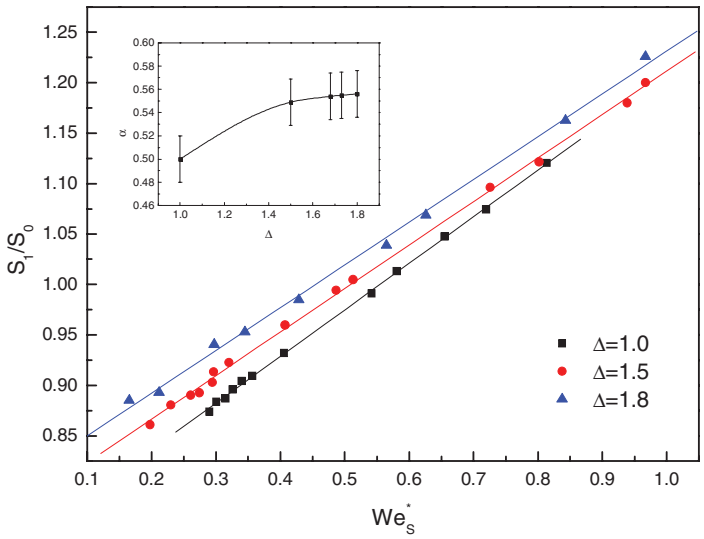

FIG. 8. (Color online) Variation of S_1 with We_s for the evaluation of viscous loss in Stage 1. Symbols are experimental data and the solid lines are the linear correlations. The inset shows the viscous dissipation coefficient α as a weak function of the size ratio.

where a, b are the principal radii of curvature and v_2 is the characteristic velocity of the surface-tension-driven flow in the disc region. The viscous loss associated with the flow is estimated by Qian and Law[11]

$$\phi_2 \sim \frac{1}{2}\mu\left(\frac{v_2}{b}\right)^2\left(\frac{a}{v_2}\right)\left(V_0 - \frac{2}{3}\pi c^3\right) = \frac{\sqrt{2}}{3}\pi\mu R_s^{3/2}\sqrt{\frac{\sigma}{\rho}}\frac{\tilde{a}^{1/2}}{\tilde{b}^2}\sqrt{1+\frac{\tilde{a}}{\tilde{b}}}\left[2(1+\Delta^3)-\tilde{c}^3\right], \quad (10)$$

where $\tilde{a} = a/R_S$, $\tilde{b} = b/R_S$, $\tilde{c} = c/R_S$. Similarly, in the bulging portion of the droplet, we can relate the characteristic velocity $v_{2'}$ with the capillary pressure $2\sigma/c$ by

$$\frac{1}{2}\rho v_{2'}^2 = \frac{2\sigma}{c}. \quad (11)$$

The corresponding viscous loss is given by

$$\phi_{2'} \sim \frac{1}{2}\mu\left(\frac{v_{2'}}{c}\right)^2\left(\frac{c}{v_{2'}}\right)\left(\frac{2}{3}\pi c^3\right) = \frac{2}{3}\pi\mu R_s^{3/2}\sqrt{\frac{\sigma}{\rho}}\tilde{c}^{3/2}. \quad (12)$$

Finally, Φ_2 can be expressed as the sum of the viscous loss ϕ_2 and $\phi_{2'}$,

$$\Phi_2 = \phi_2 + \phi_{2'}. \quad (13)$$

The viscous loss Φ_3 during Stage 3 can be evaluated by following the same approach used to estimate Φ_2. The two separated portions of the droplet, as shown in Instant 7, Figure 7, are assumed to have different characteristic flow times, which also depend on the size ratio. Specifically, the characteristic length for the larger and smaller portions are $f\Delta/(1+\Delta)/v_3$ and $f/(1+\Delta)/v_{3'}$, respectively, where v_3 and $v_{3'}$ are the corresponding characteristic flow velocities driven by the capillary pressures $2\sigma/d$ and $2\sigma/e$, respectively. Consequently, we have

$$\Phi_3 = \phi_3 + \phi_{3'}, \quad (14)$$

$$\phi_3 \sim \frac{1}{2}\mu\left(\frac{v_3}{d}\right)^2\left(f\frac{\Delta}{1+\Delta}/v_3\right)\left(\frac{4}{3}\pi\Delta^3 R_s^3\right) = \frac{4}{3}\pi\mu R_s^{3/2}\sqrt{\frac{\sigma}{\rho}}\frac{\Delta^4}{1+\Delta}\frac{\tilde{f}}{\tilde{d}^{5/2}}, \quad (15)$$

$$\phi_{3'} \sim \frac{1}{2}\mu\left(\frac{v_{3'}}{e}\right)^2\left(f\frac{1}{1+\Delta}/v_{3'}\right)\left(\frac{4}{3}\pi R_s^3\right) = \frac{4}{3}\pi\mu R_s^{3/2}\sqrt{\frac{\sigma}{\rho}}\frac{1}{1+\Delta}\frac{\tilde{f}}{\tilde{e}^{5/2}}, \quad (16)$$

where

$$v_3 = 2\sqrt{\sigma/\rho d},\ v_{3'} = 2\sqrt{\sigma/\rho e},\ \tilde{d} = d/R_S,\ \tilde{e} = e/R_S,\ \tilde{f} = f/R_S.$$

Substituting Eqs. (5), (6), (13), and (14) into (3) and non-dimensionalizing each energy term with the initial surface energy, $4\pi\sigma R_S^2(1+\Delta^2)$, we have an explicit expression for the transition Weber number $We_{\text{c-s}}$:

$$We_{c-s} = \beta Z + \gamma, \quad (17)$$

where Z is an Ohnesorge number, and β and γ are, respectively, given by

$$\beta = \frac{1}{1-\alpha}\left[\begin{array}{l}\dfrac{\tilde{a}^{1/2}}{\sqrt{2}\tilde{b}^2}\sqrt{1+\dfrac{\tilde{a}}{\tilde{b}}}\left(\dfrac{(1+\Delta^3)^2}{4\Delta^3}-\dfrac{(1+\Delta^3)\tilde{c}^3}{8\Delta^3}\right)+ \\ \dfrac{(1+\Delta^3)\tilde{c}^{3/2}}{8\Delta^3}+\dfrac{(1+\Delta^3)\tilde{f}}{4\Delta^3(1+\Delta)}\left(\dfrac{\Delta^4}{\tilde{d}^{5/2}}+\dfrac{1}{\tilde{e}^{5/2}}\right)\end{array}\right], \quad (18)$$

$$\gamma = \frac{3(S_f - S_o)(1+\Delta^3)}{(1-\alpha)\pi R_S^2\Delta^3}. \quad (19)$$

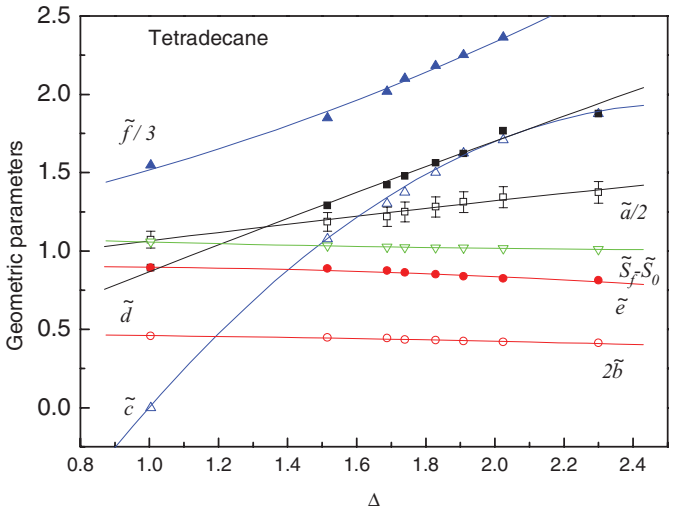

FIG. 9. (Color online) Geometric parameters as a function of the size ratio. Scatters are the experimental measurements and lines are the fitting results.

It is seen that in Eq. (17), the Weber number represents the kinetic energy, while βZ represents the viscous dissipation and γ represents the residual surface energy. In addition, Eq. (17) has exactly the same functional form as that derived by Qian and Law,[11] except that β and γ in the present problem depend on the size ratio. In the limiting case of $\Delta = 1$, Eq. (17) degenerates to that of Qian and Law.

In order to evaluate Eqs. (17)–(19), we need to determine the size-ratio dependent parameters a, b, c, d, e, f, and S_f, which depict the droplet geometry in different collision stages. In the present study, we experimentally measured these parameters at the transition Weber numbers for tetradecane droplet collision at different size ratios and then fitted them into functions of the size ratio.

Figure 9 shows the measured geometric parameters as a function of the size ratio for tetradecane droplet collision. All these measured geometric parameters were fitted into second order polynomials and the fitting constants are given in Table II. We assume that the geometric parameters are universal for different liquids and hence we can use them to develop a general criterion to predict $We_{\text{c-s}}$ for all liquids. It will be shown shortly that the present criterion with these fitted parameters also results in quantitatively satisfactory prediction of the transition Weber numbers for decane and water droplet collision.

C. Model predictions and comparison with experiments

Figure 10 shows the comparison between our model prediction and experimental measurements for tetradecane, decane, and water droplet collision. Qualitatively, the agreement for all the liquids

TABLE II. Fitting coefficients for geometric parameters.

$f(\Delta) = A_0 + A_1\Delta + A_2\Delta^2$	A_0	A_1	A_2
$\tilde{a}/2$	1.556	0.6032	− 0.0314
$2\tilde{b}$	0.47506	− 0.00508	− 0.01025
$\tilde{c}$	− 3.30844	4.12313	− 0.80968
$\tilde{d}$	− 0.01747	0.91154	− 0.02622
$\tilde{e}$	0.87656	0.06067	− 0.04016
$\tilde{f}/3$	3.09374	0.95754	0.502
$\tilde{S}_f - \tilde{S}_0$	1.13341	− 0.09298	0.01724

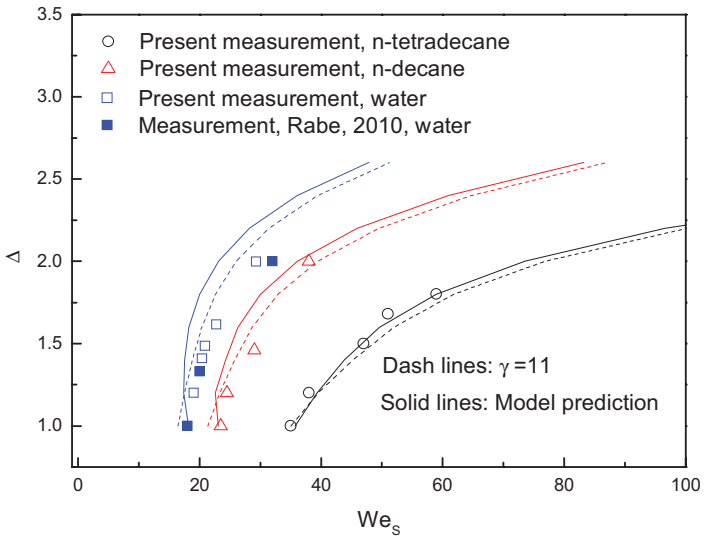

FIG. 10. (Color online) Comparison between experimentally measured and model predicted transition Weber numbers as a function of the size ratio for tetradecane, decane, and water droplet collision.

is close, showing that the transition Weber number, $We_{c\text{-}s}$, increases with the size ratio. The solid line represents the results by using the present model and the dash line presents the results by using the present model but with a constant $\gamma = 11$, which was found by Qian and Law for equal-size droplet collision. Two predictions are very close, indicating that the residual surface energy term γ in Eq. (17) is only weakly dependent on the size ratio. Quantitatively, the model predicts well tetradecane and decane droplet collision, while the discrepancy is larger for the water droplets.

In order to explain the discrepancy between the experimental results and the analysis, and to understand the underlying physics for the size-ratio dependence of $We_{c\text{-}s}$, we performed a simple sensitivity analysis on the four energy terms of Eq. (2) in the model, namely, the viscous losses Φ_1, Φ_2, Φ_3 and the residual surface energy γ. Specifically, we redid the model predictions for tetradecane, in Figure 11, by setting: (a) $\alpha = 0.5$ for all size ratios, (b) $\Phi_3 = 0$, (c) $\gamma = 0$, and (d) $\Phi_2 = 0$.

According to the model, the size-ratio dependence of Φ_1 is represented by $\alpha(\Delta)$. By setting $\alpha(\Delta) = 0.5$, the model prediction moderately shifts to smaller Weber numbers. Since α is actually larger than 0.5 and slightly increases with the size ratio, setting $\alpha = 0.5$ underestimates the viscous dissipation in Stage 1 and hence results in smaller $We_{c\text{-}s}$. Furthermore, it is seen that the role of Φ_1 is to reduce the total kinetic energy available for the merged droplet to further deform. Thus the weak size-ratio dependence of Φ_1 cannot be the primary reason for the strong size-ratio dependence of $We_{c\text{-}s}$.

By setting $\Phi_3 = 0$, the model prediction only slightly shifts to the smaller Weber number. This is due to the fact that the internal motion of the droplet in Stage 3 is slowed down after the droplet has undergone substantial viscous dissipation in Stages 1 and 2. Consequently, Φ_3 only accounts for a small portion of the total viscous loss and hence the model is also not sensitive to it.

By setting $\gamma = 0$, the model results in a much smaller prediction for $We_{c\text{-}s}$ at small size ratios, while this change almost disappears for larger size ratios. This result is consistent with the experimental observation that the residue surface area only slightly depends on the size ratio. It also implies that, with increasing size ratio, stabilization by viscous dissipation becomes dominant as compared to stabilization by surface tension.

Finally, by setting $\Phi_2 = 0$, the model prediction qualitatively disagrees with the experimental results in that $We_{c\text{-}s}$ decreases and then increases with increasing size ratio. This result therefore demonstrates that Φ_2 plays the most important role in determining the size-ratio dependence of $We_{c\text{-}s}$.

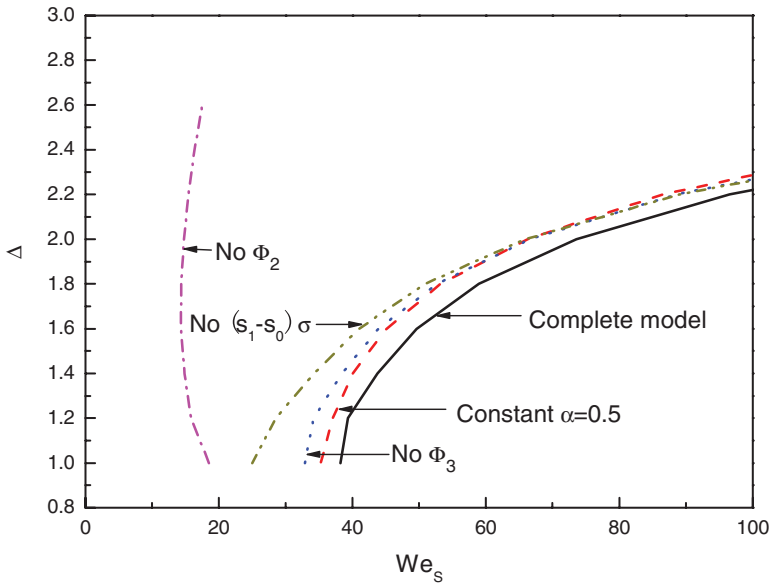

FIG. 11. (Color online) Relevancy of the present model to different energies, showing that viscous loss in Stage 2 is crucial for determining the size-ratio dependence of the transition Weber number.

To explain the substantial deficiency of the model for water droplets, we first recognize that the viscosity of water is about 40% of that of tetradecane and that its surface tension is about three times that of tetradecane. As a result, the influence of viscous dissipation, especially Φ_2, on predicting the transition Weber number for water is less significant than that for tetradecane. Furthermore, surface tension plays a more important role for water through the residue surface energy term γ than it does for tetradecane. Consequently, there is a greater extent of approximation in applying the parameter S_f-S_o, fitted for tetradecane, to a correlation for water.

We close this discussion by noting that Rabe *et al.*[13] proposed a theoretical model based on a symmetric Weber number, which combines the Weber number and the size ratio, to interpret their experimental measurement on unequal-size water droplets. The model takes into account the effects of liquid viscosity in an implicit and simplified way with a coefficient that is fitted to the experimental results for water droplets. As such, the simplified treatment for viscous dissipation in the model is not applicable to interpret the present experimental result for decane and tetradecane droplets. This difference is caused by their different viscosities. Furthermore, the reason that their model shows good agreement with both their and our experimental results on water is simply due to the small value of the Ohnesorge number, being 0.18, which implies small influence of the liquid viscosity for water, at least for the conditions investigated. Consequently, the present model is more general for head-on collisions, and as such is able to capture the essential physics of droplet collision with large deformation.

V. CONCLUDING REMARKS

The present study was motivated by the conjecture that unequal-size droplet collision holds the potential to promote permanent coalescence and subsequently the liquid-phase ignition for gelled hypergolic propellants. Our experiment first identified a unified regime diagram in terms of bouncing, coalescence, and separation for hydrocarbon and water droplets in the parameter space of the size ratio and a collision Weber number. The experimental results support our conjecture by showing that the transition Weber number, $We_{b\text{-}c}$, that separates the bouncing and coalescence regimes, weakly depends on the size ratio, and that the transition Weber number, $We_{c\text{-}s}$, that separates the coalescence and separation regimes, significantly increases with the size ratio. A theoretical model based on energy balance and scaling analysis was developed and demonstrated to predict $We_{c\text{-}s}$

well. Based on a sensitivity analysis, it is demonstrated that the strong influence of unequal-size droplet collision on suppressing droplet separation is mainly due to the increased viscous dissipation through the internal motion of the merged droplet before the droplet starts stretching to separation. The satisfactory agreement between the model prediction and the experimental observations for hydrocarbon droplets suggests that the model can be used for estimations of other hydrocarbon fuels.

ACKNOWLEDGMENTS

The work was supported by the (U.S.) Army Research Office (USARO) under the technical monitoring of Dr. Ralph Anthenien.

[1] R. Gunn, "Collision characteristics of freely falling water drops," Science **150**, 695 (1965).
[2] P. R. Brazier-Smith, S. G. Jennings, and J. Latham, "The interaction of falling water drops: Coalescence," Proc. R. Soc. London, Ser. A **326**, 393 (1972).
[3] F. Raes and R. Van Dingenen, "Simulations of sondensation and cloud condensation nuclei from biogenic So2 in the remote marine boundary-layer," J. Geophys. Res. **97**, 12901, doi:10.1029/92JD00961 (1992).
[4] F. Raes, R. Van Dingenen, E. Vignati, J. Wilson, J.-P. Putaud, J. H. Seinfeld, and P. Adams, "Formation and cycling of aerosols in the global troposphere," Atmos. Environ. **34**, 4215 (2000).
[5] H. Hiroyasu and T. Kadota, Fuel Droplet Size Distribution in Diesel Combustion Chamber, SAE, No. 740715, 1974.
[6] G. M. Faeth, "Current Status of Droplet and Liquid Combustion," Prog. Energy Combust. Sci. **3**, 191 (1977).
[7] J. R. Adam, N. R. Lindblad, and C. D. Hendrick, "Collision coalescence and disruption of water droplets," J. Appl. Phys. **39**, 5173 (1968).
[8] R. H. Magarvey and J. W. Geldart, "Drop collisions under conditions of free fall," J. Atmos. Sci. **19**, 107 (1962).
[9] C. E. Abbott, "Survey of waterdrop interaction experiments," Rev. Geophys. **15**, 363, doi:10.1029/RG015i003p00363 (1977).
[10] Y. J. Jiang, A. Umemura, and C. K. Law, "An experimental investigation on the collision behavior of hydrocarbon droplets," J. Fluid Mech. **234**, 171 (1992).
[11] J. Qian and C. K. Law, "Regimes of coalescence and separation in droplet collision," J. Fluid Mech. **331**, 59 (1997).
[12] N. Ashgriz and J. Y. Poo, "Coalescence and separation in binary collisions of liquid-drops," J. Fluid Mech. **221**, 183 (1990).
[13] C. Rabe, J. Malet, and F. Feuillebois, "Experimental investigation of water droplet binary collisions and description of outcomes with a symmetric Weber number," Phys. Fluids **22**, 047101 (2010).
[14] M. R. Nobari, Y. J. Jan, and G. Tryggvason, "Head-on collision of drops - A numerical investigation," Phys. Fluids **8**, 29 (1996).